# SAND REPORT

SAND2006-6950
Unlimited Release
Printed November 2006

# Reduced-Volume Antennas with Integrated High-Impedance Electromagnetic Surfaces

Michael A. Forman

Prepared by
Sandia National Laboratories
Albuquerque, New Mexico 87185 and Livermore, California 94550

Sandia is a multiprogram laboratory operated by Sandia Corporation,
a Lockheed Martin Company, for the United States Department of Energy's
National Nuclear Security Administration under Contract DE-AC04-94-AL85000.



Issued by Sandia National Laboratories, operated for the United States Department of Energy by Sandia Corporation.



Available to DOE and DOE contractors from
U.S. Department of Energy
Office of Scientific and Technical Information
P.O. Box 62
Oak Ridge, TN 37831

| | |
|---|---|
| Telephone: | (865) 576-8401 |
| Facsimile: | (865) 576-5728 |
| E-Mail: | reports@adonis.osti.gov |
| Online ordering: | http://www.doe.gov/bridge |

Available to the public from
U.S. Department of Commerce
National Technical Information Service
5285 Port Royal Rd
Springfield, VA 22161

| | |
|---|---|
| Telephone: | (800) 553-6847 |
| Facsimile: | (703) 605-6900 |
| E-Mail: | orders@ntis.fedworld.gov |
| Online ordering: | http://www.ntis.gov/help/ordermethods.asp?loc=7-4-0#online |

SAND2006-6950
Unlimited Release
Printed November 2006

# Reduced-Volume Antennas with Integrated High-Impedance Electromagnetic Surfaces

Michael A. Forman
Multiphysicis Modeling and Simulation
Sandia National Laboratories
P.O. Box 969
Livermore, CA 94551-0969 USA
Michael.A.Forman@Sandia.GOV

**Abstract**

Several antennas with integrated high-impedance surfaces are presented. The high-impedance surface is implemented as a composite right/left-handed (CRLH) metamaterial fabricated from a periodic structure characterized by a substrate, filled with an array of vertical vias and capped by capacitive patches. Omnidirectional antennas placed in close proximity to the high-impedance surface radiate hemispherically with an increase in boresight far-field pattern gain of up to 10 dB and a front-to-back ratio as high as 13 dB at 2.45 GHz. Several TEM rectangular horn antennas are realized by replacing conductor walls with high-impedance surfaces. The TEM horn antennas are capable of operating below the $TE_{1,0}$ cutoff frequency of a standard all-metal horn antenna, enabling a reduction in antenna volume. Above the cutoff frequency the TEM horn antennas function similarly to standard rectangular horn antennas.

# Acknowledgment

The author thanks Troy Satterthwait for his exceptional management and coordination of the test-and-measurement facilities. Thanks to George Audycki whose late-night fabrication efforts allowed the incorporation of last-minute design changes. This work was funded under LDRD 06-1039. Sandia is a multiprogram laboratory operated by Sandia Corporation, a Lockheed Martin Company, for the United States Department of Energy's National Nuclear Security Administration under contract DE-AC04-94AL85000.

# Contents



# Figures



# Tables

This page intentionally left blank

# Reduced-Volume Antennas with Integrated High-Impedance Electromagnetic Surfaces

## Introduction

Due to the miniaturization of wireless systems, antennas are being reduced in volume and placed in close proximity to other system elements. In these configurations novel topologies are required to both maximize gain and minimize near-field coupling. Antennas incorporating Sievenpiper high-impedance electromagnetic surfaces [1] are capable of providing such performance improvements and thus enabling reductions in volume [2] and flexible methods of deployment.

A high-impedance surface (HIS) is an electrically thin in-phase reflector which provides surface-wave suppression. Within a given frequency band the currents from a near-by antenna and its image are in phase, as opposed to being 180° out of phase as with standard conductors. Furthermore, because surface waves are suppressed, power loss through the dielectric is minimized. These two properties result in a net increase in radiation efficiency from the use of a HIS as compared to a standard conductor.

A Sievenpiper high-impedance surface is implemented by means of a via array in a dielectric with capacitive patches on top. The vias and patches provide lumped-circuit equivalents that are modeled as a parallel resonant circuit. The geometry and thus the lumped-circuit equivalents are tuned to exhibit a high impedance over a predetermined frequency band. This structure is not a photonic band gap (PBG) material, in that it does not suppress surfaces waves through Bragg scattering from a periodic unit cell, thus unit cells can be a fraction of the free-space wavelength. The structure is instead a composite right/left-handed (CRLH) metamaterial whose subwavelength unit cells act as a homogeneous effective dielectric.

In the following work two antenna topologies are presented. The first topology places an omnidirectional monopole, stub, and chip antenna in close proximity to a high impedance surface. The goal is to enable the placement of omnidirectional radiators in close proximity to conductors, while maintaining or improving the insertion loss and far-field pattern. The second topology employs high-impedance surfaces as the walls of a rectangular horn antenna. The goal is to allow the antenna to function as a TEM waveguide at dimensions that would otherwise be below the $TE_{1,0}$ cutoff frequency, thus enabling a reduction in antenna volume.

A common high-impedance surface is designed for both the reflector and the TEM horn antennas. A single substrate is designed to be placed in close proximity to three different omnidirectional antennas. Finally, four different horn antennas comprised of probe-fed rectangular waveguides with high-impedance surfaces as sides are also designed.

# High-Impedance Surface

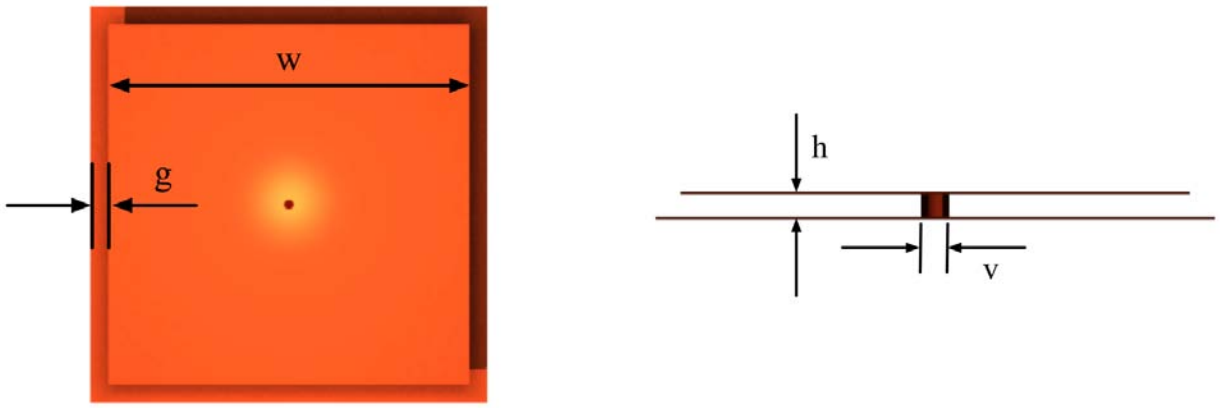


(a) (b)

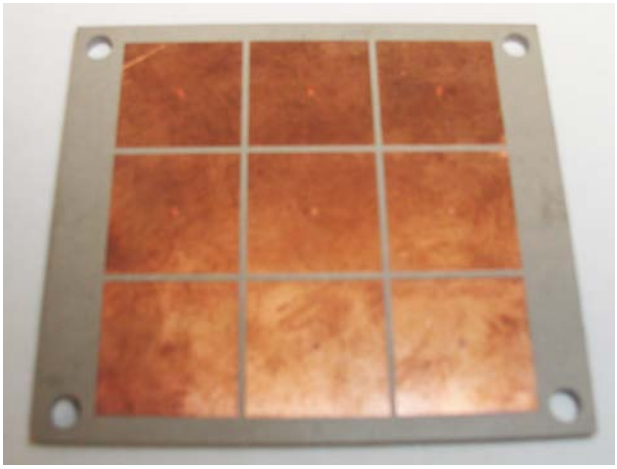

(c)

**Figure 1.** High-impedance surface as seen from the top (a) and side (b) with important dimensions labeled. For clarity, the substrate, which resides between the top and bottom patches of metal, is omitted. A fabricated three-by-three unit-cell array (c) used in reflection measurements.

Surface impedance can be modeled as a parallel resonant circuit that is tuned to exhibit high impedance over a predetermined frequency band [1]. In reference to the geometry shown in Figure 1, fringing electric fields between adjacent top patches can be represented as a capacitance and

**Table 1.** Design parameters for the high-impedance surface.

| Parameter | Value |
|---|---|
| Substrate | RT/Duriod 6006 |
| $e_r$ | 6.15 |
| $h$ | 2.54 mm |
| $t$ | 8.5 µm |
| $w$ | 18.2 mm |
| $g$ | 1.0 mm |
| $v$ | 1.0 mm |
| $f_0$ | 2.45 GHz |

magnetic fields in the dielectric generated by current through the vias and ground can be represented as an inductance. A sheet impedance can be defined to be equal to the impedance of the equivalent parallel resonant circuit

$$Z = \frac{j\omega L}{1-\omega^2 LC}. \tag{1}$$

High impedance occurs near the resonant frequency, $\omega_0$, where

$$\omega_0 = \frac{1}{\sqrt{LC}}. \tag{2}$$

This frequency marks the center of the high-impedance surface's forbidden frequency bandgap.

At frequencies far from the resonant frequency the high-impedance surface behaves like a conductor. Thus an antenna in parallel with the surface will be mirrored by an opposing current on the surface, reducing its radiation efficiency. At the resonant frequency an antenna lying parallel will be mirrored by an in-phase current on the surface, increasing its radiation efficiency.

The bandwidth of the high-impedance region is defined as the frequencies, where the radiation drops to half of its maximum value and occurs where the surface impedance is equal to the impedance of free space. For normal radiation, one has the following equation

$$\left| \frac{j\omega L}{1-\omega^2 LC} \right| = \eta. \tag{3}$$

Solving for $\omega$, eliminating higher-order terms in light of realistic values of $L$ and $C$, and, given that $Z_0 << \eta$, the stop band can be approximated by

$$\omega = \omega_0 \left( 1 \pm \frac{1}{2} \frac{Z_0}{\eta} \right), \tag{4}$$

which is the range, over which an antenna radiates efficiently on a high-impedance surface. The total bandwidth is approximately equal to the characteristic impedance of the surface divided by the impedance of free space. This is the bandwidth over which the reflection coefficient falls between $\pm 90^\circ$ and represents the maximum usable bandwidth for a parallel antenna over a resonant surface.

The surface fabricated in the following work is designed using previously published values [3, 4] to operate at 2.45 GHz and simulated to verify performance. The substrate is fabricated

on Rogers RT/Duroid 6006, with a unit cell approximately 20 mm ($\lambda/6$) square. The simulated bandwidth is 12 %. Values are summarized in Table 1 and the fabricated substrate is shown in Figure 1(c).

# High-Impedance Reflector

Metallic sheets are used in many antenna configurations as reflectors to direct radiation and provide shielding [5]. Because image and antenna currents are 180° out of phase, antenna-ground separation must be a multiple of $\lambda/4$, to prevent low radiation efficiency. A high-impedance surface can be used in place of or in front of a metallic ground plane, allowing close placement of the antenna and ground, thus reducing the required volume and enabling novel configurations. Additionally, omnidirectional radiators can be converted to directional radiators and thus situated near metallic structures with the addition of a high-impedance surface. Because reflections from a high-impedance surface are in phase, they are sometimes called magnetic conductors. Another property of metallic sheets is that they support surface waves [6, 7]. A surface wave is a propagating electromagnetic wave that is bound to the interface between metal and free space. Surface waves contribute to far-field pattern sidelobes and can increase near-field coupling for antennas sharing a common substrate. The use of a high-impedance surface eliminates surface waves.

## Design

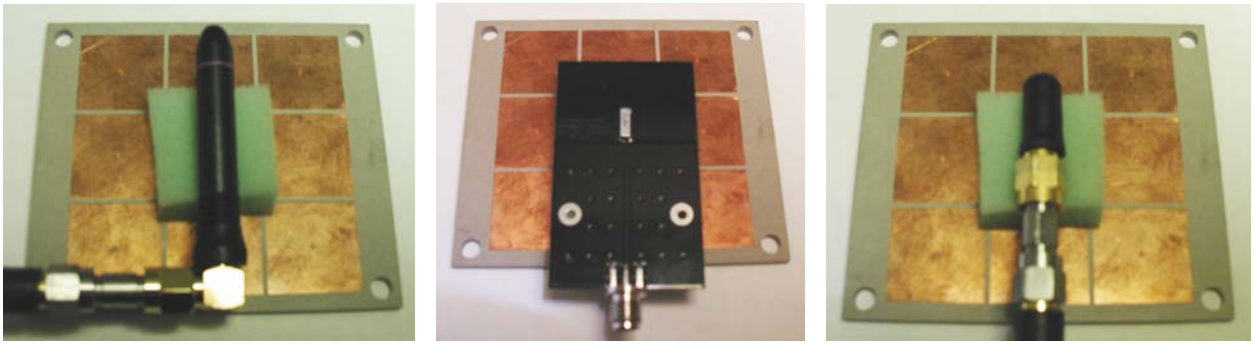

(a) (b) (c)

**Figure 2.** Images of the quarter-wave antenna (a), LTCC chip antenna (b), and helical stub antenna (c) over a high-impedance surface.

A high-impedance reflector is implemented as an omnidirectional antenna positioned parallel to a high-impedance surface [8]. The high-impedance surface is a three-by-three array of unit cells, measuring approximately 60 mm × 60 mm ($\lambda/2 \times \lambda/2$), as seen in Figure 1(c). Three antennas selected for measurement in the reflector configuration are manufactured by *Antenna Factor* and

**Table 2.** Antenna specifications for reflection measurements.

| Antenna Model | Dimensions | Description |
|---|---|---|
| ANT-2.4-CW-RCS | 9.4 mm × 54 mm | Quarter-wave antenna |
| ANT-2.4-CHP-T | 2.2 mm × 6.5 mm | LTCC chip antenna |
| ANT-2.4-CW-RH-SMA | 7.4 mm × 8.4 mm | Helical stub antenna |

are specified in Table 2 and shown in Figure 2. The antennas are held approximately 10 mm above the high-impedance surface by foam.

## Measurements

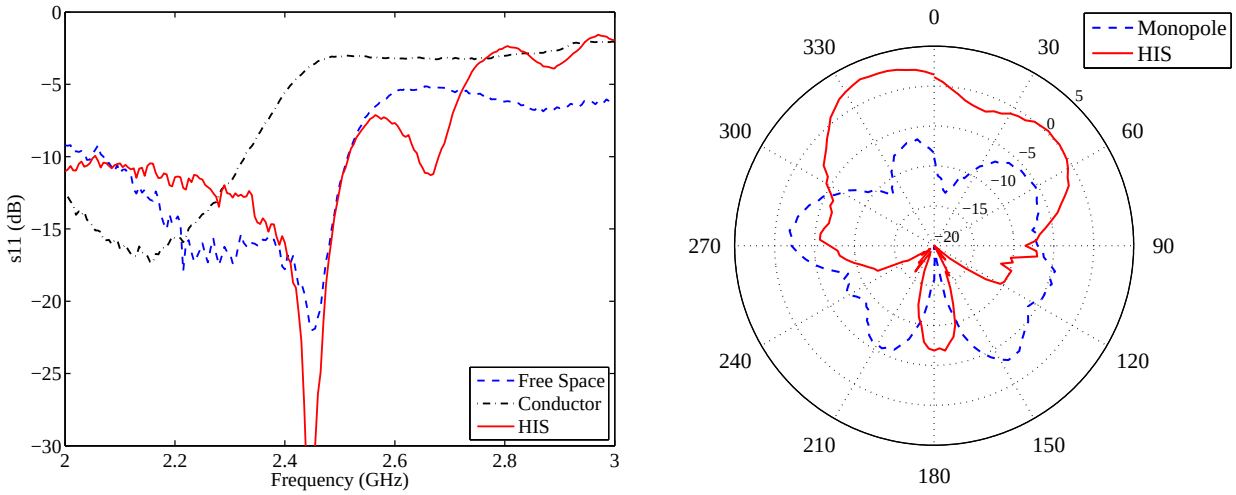


**Figure 3.** Measured insertion loss (a) and H-plane far-field patterns (b) for a quarter-wave antenna with and without a backing high-impedance surface.

The insertion loss and far-field pattern for the quarter-wave antenna are shown in Figure 3. The insertion loss is measured approximately 10 mm above a high-impedance surface, 10 mm above a ground plane, and without a loading surface. It can be seen in Figure 3(a) that insertion loss provided by the high-impedance surface is 30 dB lower than the conductor backing and 14 dB lower than an unloaded antenna. Antenna gain in the boresight direction, normal to the high-impedance surface is approximately 3 dBi, up 10 dB relative to omnidirectional, with a front-to-back ratio of 10 dB. Far-field pattern measurements are performed at 2.45 GHz.

The insertion loss and far-field pattern for the chip antenna are shown in Figure 4. The insertion loss is measured 10 mm above a high-impedance surface, 10 mm above a ground plane, and without

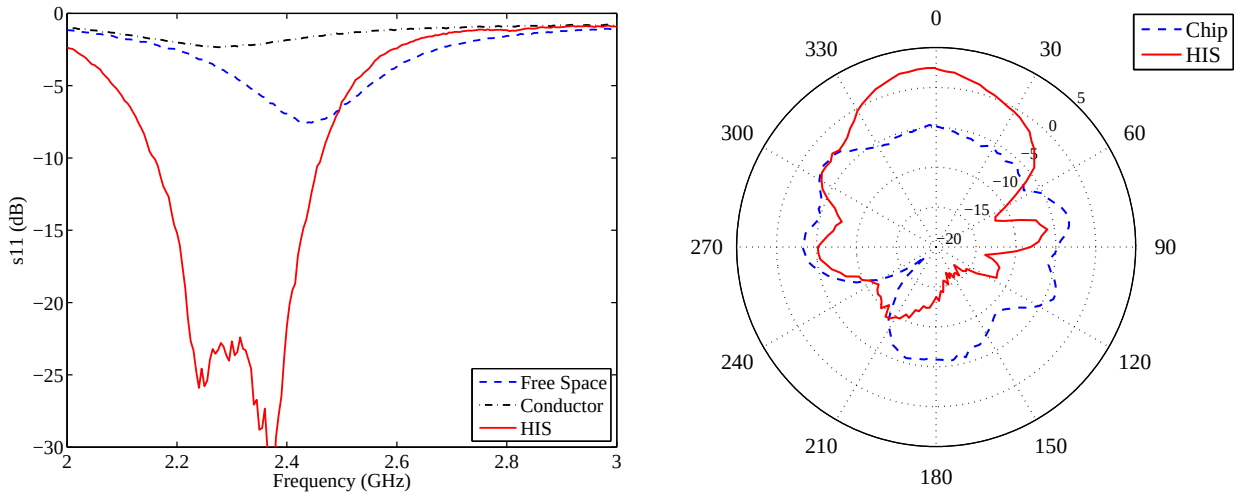


(a) (b)

**Figure 4.** Measured insertion loss (a) and H-plane far-field patterns (b) for a chip antenna with and without a backing high-impedance surface.

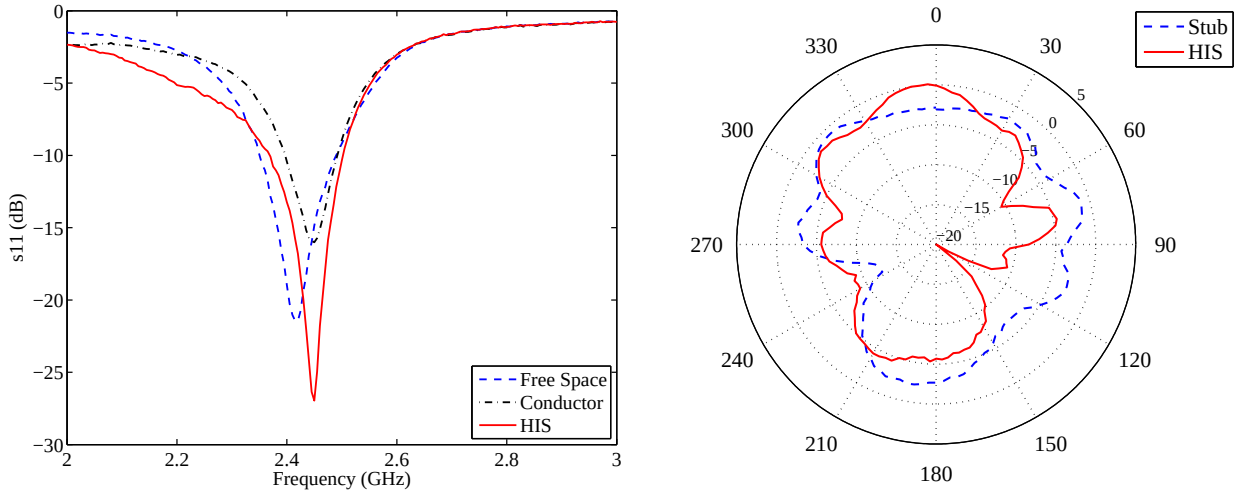


(a) (b)

**Figure 5.** Measured insertion loss (a) and H-plane far-field patterns (b) for a stub antenna with and without a backing high-impedance surface.

a loading surface. Insertion loss provided by the high-impedance surface is 30 dB lower than the conductor backing and 25 dB lower than an unloaded antenna. The 2:1 VSWR bandwidth has increased to 15 %. Antenna gain in the boresight direction is approximately 3 dBi, up 8 dB relative to omnidirectional, with front-to-back ratio of 13 dB.

The insertion loss and far-field pattern for the quarter-wave antenna are shown in Figure 5. The insertion loss is measured 10 mm above a high-impedance surface, 10 mm above a ground plane, and without a loading surface. It can be seen that insertion loss provided by the high-impedance surface is 12 dB lower than the conductor backing and 5 dB lower than an unloaded antenna. Antenna gain is only slightly changed. It is believed, because the currents on a helical antenna travel only partially in plane with the high-impedance surface, that the increase in far-field pattern gain is reduced relative to the preceding antennas.

Qualitatively, the high-impedance surface has a positive effect on the antenna match, providing lower insertion loss and wider bandwidths in all cases. The measured commercial antennas respond favorably to the presence of a high-impedance surface and are easy to tune.

# TEM Horn Antenna

From basic electromagnetics it is well known that the transverse dimension of a waveguide must be at least one half wavelength. For such a geometry the field distribution satisfies the boundary conditions needed for the propagation of the electromagnetic wave along the waveguide. To miniaturize a rectangular waveguide, traditionally one would fill it with a dielectric, where the transverse dimension would decrease by the square root of the relative permittivity. Due to dielectric loss, difficulty in manufacturing, and maximum permittivities, this approach has limits. The use of high-impedance surfaces for waveguide walls, however, allows TEM propagation, eliminating cutoff frequencies and allowing arbitrary reduction in waveguide size [9, 10]. With the use of high-impedance surfaces a TEM horn antenna and feed can be designed that will operate below traditional cutoff frequencies, thus allowing the arbitrary reduction in antenna volume.

Rectangular waveguides with uniform field distributions are employed in quasioptical power combining [11]. It has been shown that a photonic band-gap (PBG) structure can be used to build a TEM waveguide with a uniform field distribution by placing the side walls with PBG structures [9]. The resulting magnetic boundary condition generates a TEM parallel-plate mode. This work seeks to build upon these previous results by replacing the PBG structure with a metamaterial high-impedance surface with a smaller unit-cell size. The goal is to implement a rectangular horn antenna that would otherwise be so small that it would be in cutoff, if operating in TE or TM mode.

## Design

Several rectangular horn antennas are measured with both high-impedance and standard-metallic walls to compare insertion losses, far-field patterns, and cutoff frequencies. The horn antennas are assembled from components of machined aluminum and high-impedance surface and secured in

**Table 3.** Horn identifiers, dimensions, and $TE_{1,0}$ cutoff frequencies.

| H11 | H31 |
|---|---|
| $h = 20\,\text{mm}$ | $h = 60\,\text{mm}$ |
| $w = 20\,\text{mm}$ | $w = 20\,\text{mm}$ |
| $f_c = 7.5\,\text{GHz}$ | $f_c = 2.5\,\text{GHz}$ |
| H13 | H33 |
| $h = 20\,\text{mm}$ | $h = 60\,\text{mm}$ |
| $w = 60\,\text{mm}$ | $w = 60\,\text{mm}$ |
| $f_c = 7.5\,\text{GHz}$ | $f_c = 2.5\,\text{GHz}$ |

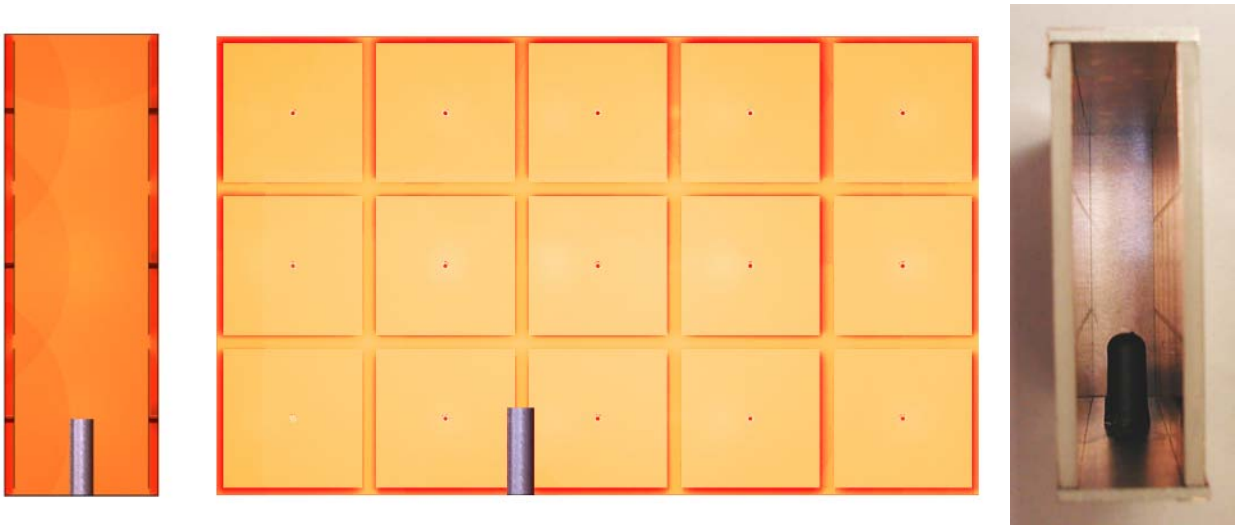

(a) (b) (c)

**Figure 6.** H13 horn schematic shown from the front (a) and side cutaway (b). Fabricated H13 horn is shown (c).

various configurations with copper tape. The top, bottom, and back of the antennas are aluminum and the sides are either aluminum or high-impedance surface. The bottom aluminum plate has a narrow channel to allow for the tuning of an inserted feed antenna. After tuning the feed is fixed and the channel is covered with copper tape.

To facilitate fabrication, the dimensions of the walls of the horn antennas are chosen to be integer multiples of a unit cell's width, which is approximately 20 mm. Components based on one and three multiples of a unit cell are fabricated, providing four geometries of $1\times1$ (H11), $1\times3$ (H13), $3\times1$ (H31), and $3\times3$ (H33) in both TE/TM and TEM configurations for a total of eight configurations. All configurations are five unit cells or 100 mm ($0.833\lambda$) deep. These geometries set the $TE_{1,0}$ cutoff frequency of the metallic-walled antennas to either 2.5 GHz and 7.5 GHz as shown in (Table 3). Images of the H13 horn are shown in Figure 6.

## Measurements

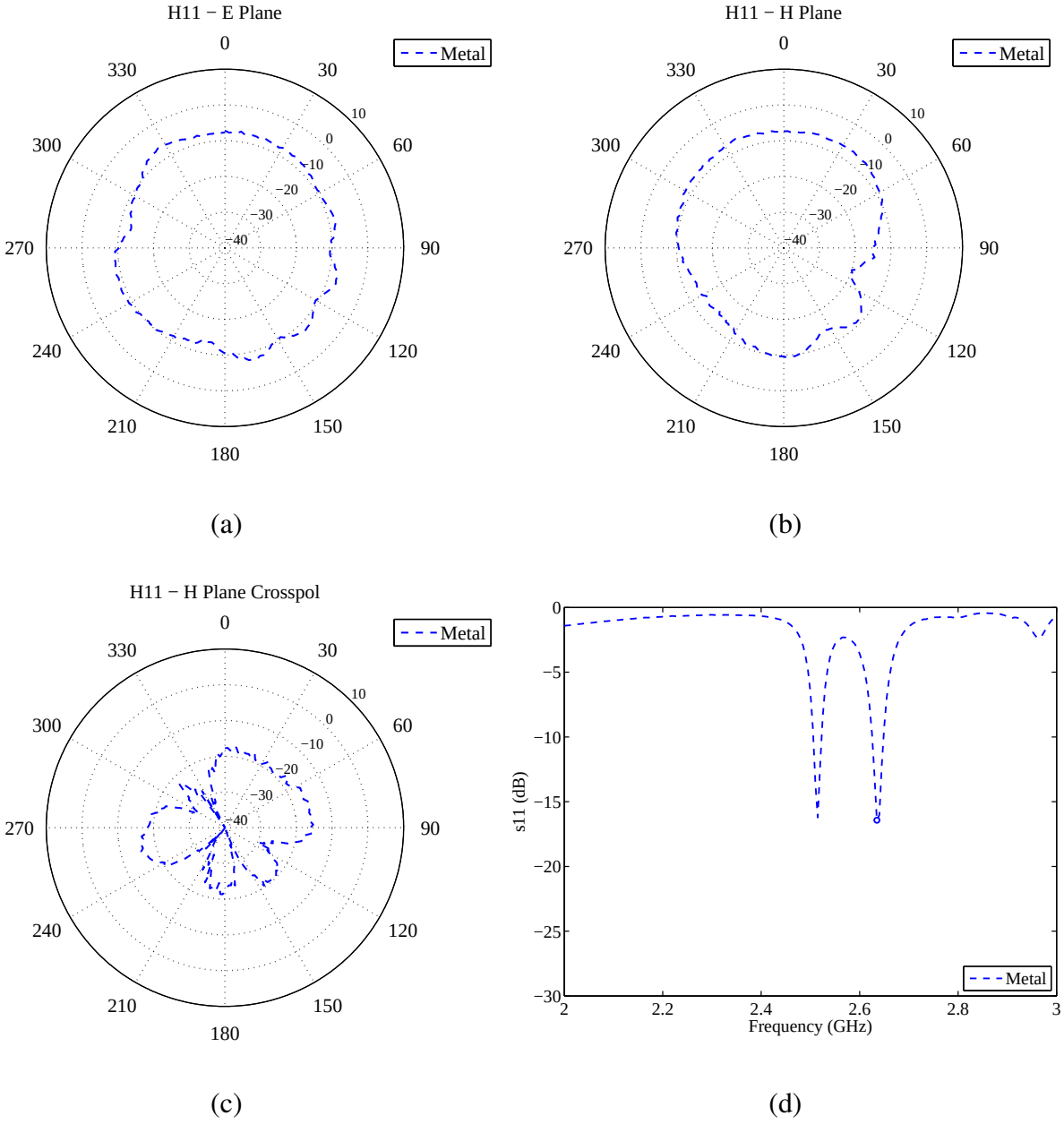


**Figure 7.** Measured E-Plane (a), H-Plane (b), and H-Plane cross polarization (c) far-field patterns. Insertion loss (d) for the H11 horn antenna.

A stub feed is inserted into each antenna, tuned, and fixed. An *Agilent* E8361A Network Analyzer is employed to measure insertion loss and principal-plane far-field pattern measurements in an anechoic chamber at 2.5 GHz. The insertion loss and far-field pattern of the H11 rectangular horn are shown in Figure 7. The H11 rectangular horn is one unit cell wide and one unit cell

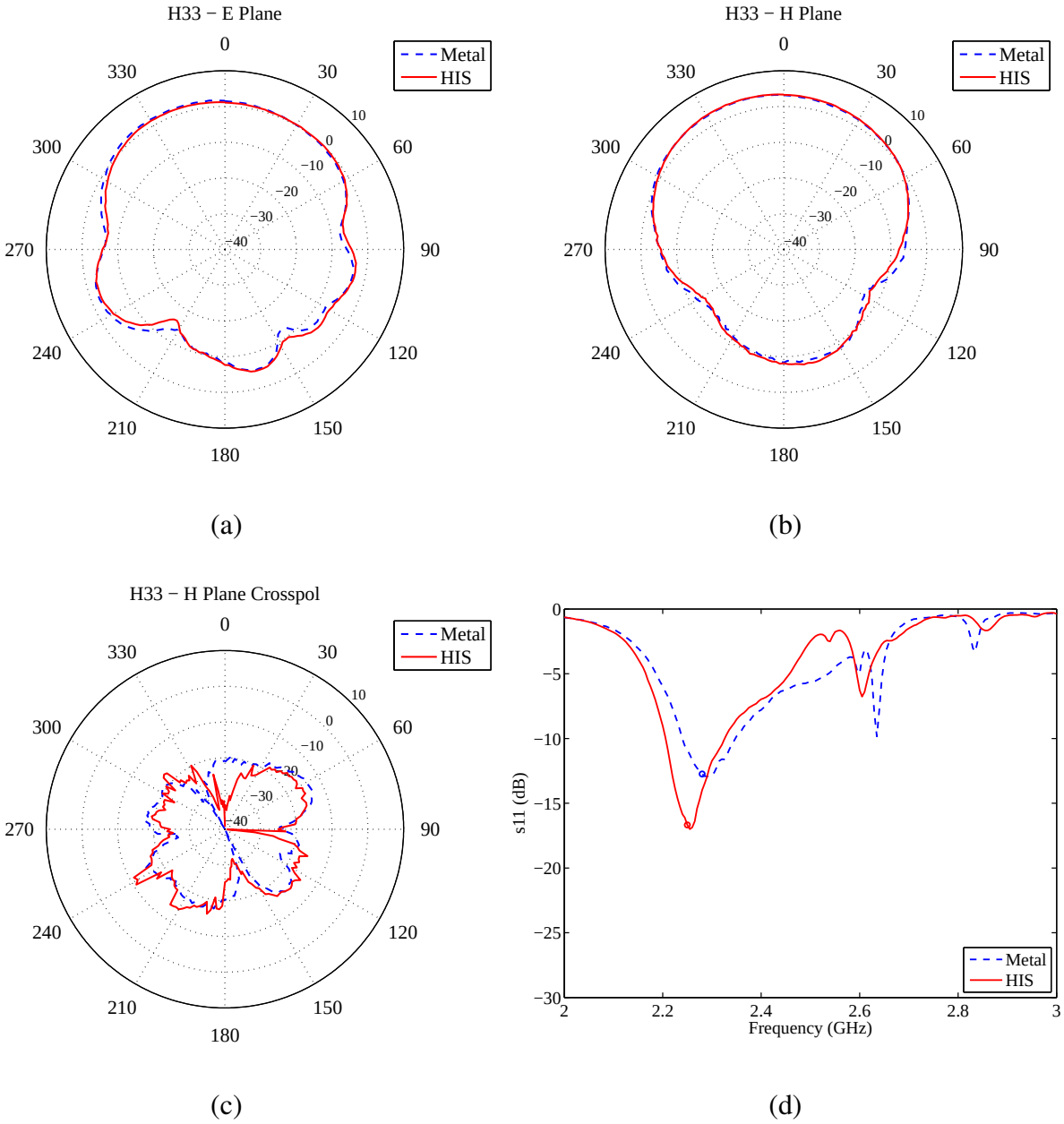


**Figure 8.** Measured E-Plane (a), H-Plane (b), and H-Plane cross polarization (c) far-field patterns. Insertion loss (d) for the H33 horn antenna.

tall (20 mm × 20 mm) and has a cutoff frequency of 7.5 GHz. This particular horn configuration can not be implemented with high-impedance surface walls, as at least two vertical unit cells separated by a gap are required to provide the necessary capacitance. Because of this, only a single measurement for metallic walls is shown. As can be seen by the low gain (-9 dBi) the rectangular horn antenna is operating below it cutoff frequency.

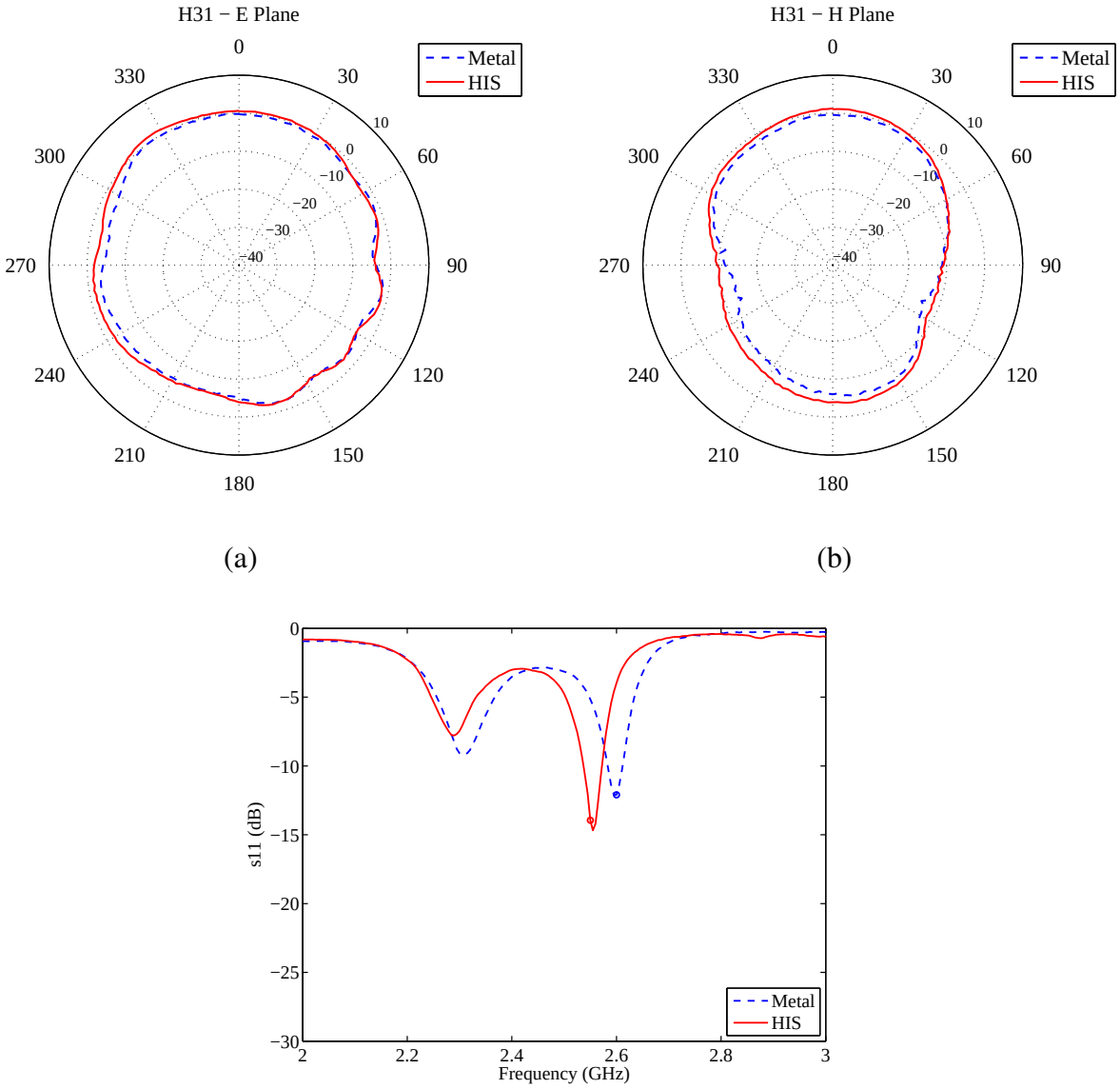


**Figure 9.** Measured E-Plane (a) and H-Plane (b) far-field patterns. Insertion loss (c) for the H31 horn antenna.

The insertion loss and far-field pattern of the H33 rectangular horn are shown in Figure 8. The H33 rectangular horn is three unit cells wide and three unit cells tall (60 mm × 60 mm) and is measured just above its cutoff frequency of 2.5 GHz. As can be seen in the insertion loss and far-field pattern measurements, the metallic- and HIS-walled antennas perform similarly.

The insertion loss and far-field pattern of the H31 rectangular horn are shown in Figure 9. The H31 rectangular horn is three unit cells wide and one unit cell tall (60 mm × 20 mm) and is measured just above its cutoff frequency of 2.5 GHz. As can be seen in the insertion loss and

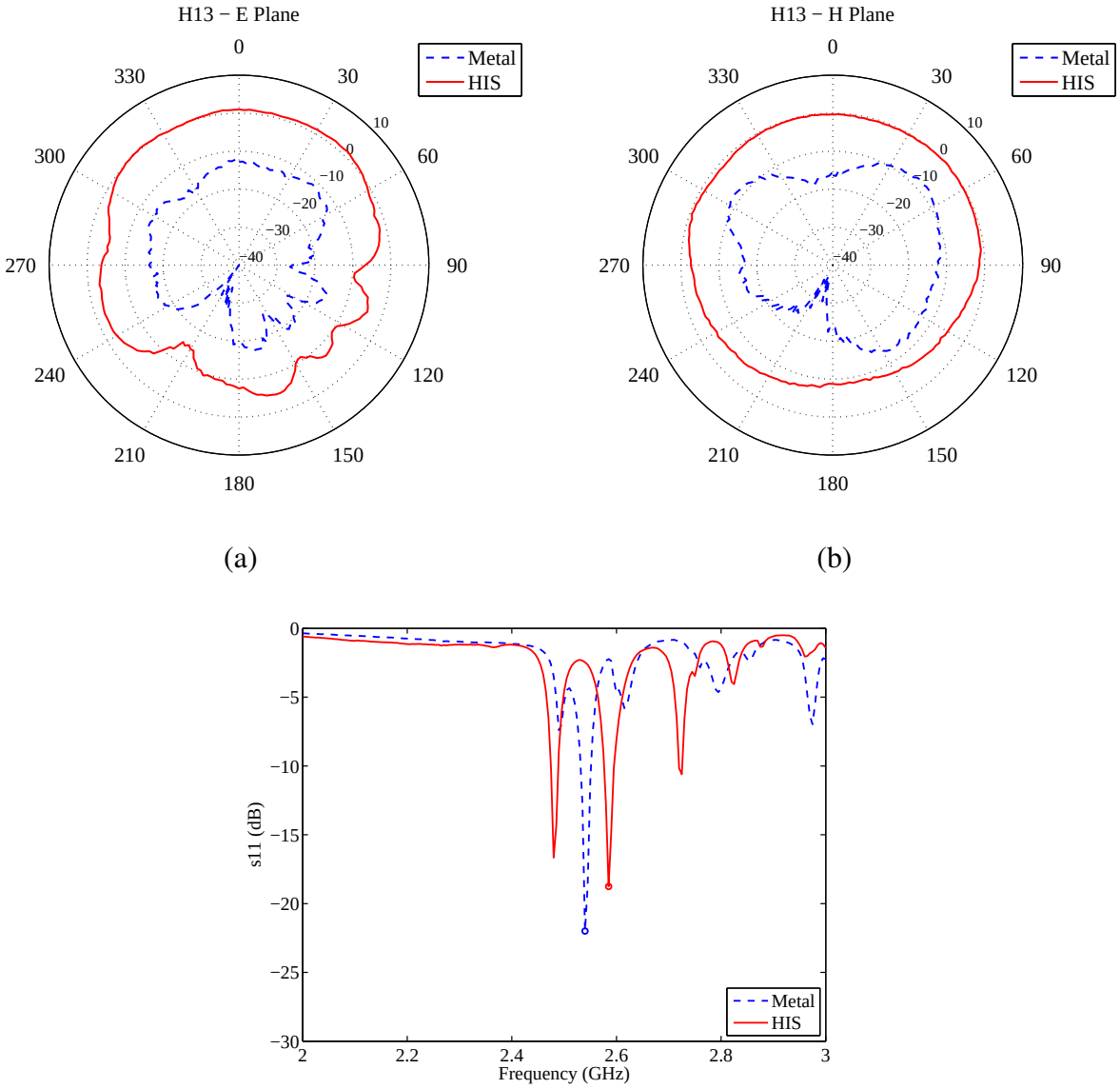


**Figure 10.** Measured E-Plane (a) and H-Plane (b) far-field patterns. Insertion loss (c) for the H13 horn antenna.

far-field pattern measurements, the metallic- and HIS-walled antennas perform similarly.

The insertion loss and far-field pattern of the H13 rectangular horn are shown in Figure 10. The H13 rectangular horn is one unit cell wide and three unit cells tall (20 mm × 60 mm) and has a cutoff frequency of 7.5 GHz. As can be seen in the insertion loss and far-field pattern measurements, the metallic-walled antenna is in cutoff, whereas the antenna with the high-impedance surfaces as walls is not. This demonstrates that the antenna with the high-impedance surfaces as walls is operating in TEM mode. The use of TEM-mode rectangular waveguides and antennas provides

similar functionality of standard rectangular waveguides in a reduced volume.

# Conclusions

Omnidirectional antennas placed in close proximity to a high-impedance surface have been shown to radiate hemispherically with an increase in boresight far-field pattern gain of up to 10 dB and a front-to-back ratio as high as 13 dB at 2.45 GHz. Further, several TEM rectangular horn antennas have been realized by replacing conductor walls with high-impedance surfaces. The TEM horn antennas are capable of operating below the $TE_{1,0}$ cutoff frequency of a traditional all-metal horn antenna, enabling a reduction in antenna volume. Above the cutoff frequency the TEM horn antennas function similarly to standard rectangular horn antennas.

# References


[1] D. Sievenpiper, L. Zhang, R. Jimenez Broas, N. Alexópolous, and E. Yablonovitch, "High-impedance electromagnetic surfaces with a forbidden frequency band," *IEEE Transactions on Microwave Theory and Techniques*, vol. 47, no. 11, 1999.

[2] S. Hrabar, J. Bartolic, and Z. Sipus, "Waveguide miniaturization using uniaxial negative permeability metamaterial," *IEEE Transactions on Antennas and Propagation*, vol. 53, pp. 110–119, jan 2005.

[3] J. R. Sohn, H. Tae, J. Lee, and J. Lee, "Comparative analysis of four types of high-impedance surfaces for low profile antenna applications," *IEEE Antennas and Propagation Society International Symposium*, vol. 1A, pp. 758–761, jul 2005.

[4] S. Clavijo, R. E. Diaz, and W. E. McKinzie III, "Design methodology for sievenpiper high-impedance surfaces: an artificial magnetic conductor for positive gain electrically small antennas," *IEEE Transactions on Antennas and Propagation*, vol. 51, pp. 2678–2690, oct 2003.

[5] Constantine A. Balanis, *Antenna Theory: Analysis and Design*, chapter 1, Harper & Row, New York, 1982.

[6] S. Ramo, J. Whinnery, and T. Van Duzer, *Fields and Waves in Communication Electronics*, John Wiley & Sons, Inc., New York, NY, 1984.

[7] R. Collin and, *Field Theory of Guided Waves*, IEEE Press, New York, NY, 1991.

[8] R. F. J. Broas, D. F. Sievenpiper, and E. Yablonovitch, "A high-impedance ground plane applied to a cellphone handset geometry," *IEEE Transactions on Microwave Theory and Techniques*, vol. 49, pp. 1262–1265, jul 2001.

[9] F. Yang, K. Ma, Y. Qian, and T. Itoh, "A novel tem-waveguide using uniplanar compact photonic band-gap (uc-pbg) structure," *Asia Pacific Microwave Conference*, vol. 2, pp. 323–326, 1999.

[10] J. A. Higgins, H. Xin, and A. Sailer, "Characteristics of Ka band waveguide using electromagnetic crystal sidewalls," *IEEE MTT-S International Microwave Symposium Digest*, vol. 2, pp. 1071–1074, jun 2002.

[11] Robert A. York, "Quasi-optical power combining," in *Active and Quasi-optical arrays for solid-state power combining*, Robert A. York and Zoya B. Popović, Eds., chapter 1. John Wiley, New York, 1997.

# Distribution

| | | | | |
|---|---|---|---|---|
| 1 | MS1152 | W. A. Johnson | 1652 | |
| 1 | MS0986 | R. J. Franco | 2664 | |
| 1 | MS0986 | R. A. Bates | 2664 | |
| 1 | MS1332 | S. E. Allen | 5345 | |
| 1 | MS0529 | K. C. Branch | 5345 | |
| 1 | MS0529 | B. C. Brock | 5345 | |
| 1 | MS0529 | T. V. Satterthwait | 5345 | |
| 1 | MS0529 | M. D. Sena | 5345 | |
| 1 | MS1330 | B. H. Strassner II | 5345 | |
| 1 | MS0537 | L. M. Feldner | 5353 | |
| 1 | MS0537 | C. T. Rodenbeck | 5353 | |
| 1 | MS9106 | R D. Kyker | 8226 | |
| 1 | MS9102 | K. J. Condreva | 8233 | |
| 1 | MS9102 | C. M. Haagen | 8235 | |
| 1 | MS9102 | D. I. Koida | 8235 | |
| 1 | MS9102 | R. J. Punnoose | 8235 | |
| 1 | MS9102 | J. F. Stamps | 8235 | |
| 1 | MS9102 | K. Wallace | 8235 | |
| 1 | MS9001 | P. J. Hommert | 8000 | Attn: |
| | MS9004 | J. M. Hruby | 8100 | |
| | MS9054 | T. A. Michalske | 8300 | |
| | MS9002 | P. N. Smith | 8500 | |
| | MS9151 | L. M. Napolitano | 8900 | |
| 1 | MS9405 | R. W. Carling | 8700 | |
| 1 | MS9404 | D. M. Kwon | 8770 | |
| 1 | MS9042 | M. L. Chiesa | 8774 | |
| | MS9153 | K. C. Knapp | 8200 | |
| 1 | MS9102 | R. G. Miller | 8230 | |
| 1 | MS9102 | P. Y. Yoon | 8235 | |
| 5 | MS9102 | M. A. Forman | 8774 | |
| 2 | MS9018 | Central Technical Files | 8944 | |
| 2 | MS0899 | Technical Library | 4536 | |

This page intentionally left blank